ELSEVIER

Coordination Chemistry Reviews 230 (2002) 65–78

COORDINATION CHEMISTRY REVIEWS

www.elsevier.com/locate/ccr

Quantum chemistry and Dick Stufkens photochemistry

Chantal Daniel *

Laboratoire de Chimie Quantique, Université Louis Pasteur, UMR 7551 CNRS, 4 Rue Blaise Pascal, 67000 Strasbourg, France

Received 15 August 2001; accepted 11 January 2002

Contents

Abstract

A survey of the quantum chemical results obtained for several MLCT complexes studied in Amsterdam is presented in order to illustrate the progress made in this field from the beginning of the 1980s when excited states properties were analyzed in terms of bonding and antibonding molecular orbitals (MO). Nowadays the photoactive states and the main features of the absorption spectra can be determined without any ambiguity. The time scales of elementary processes such as direct ultra-fast dissociations or intersystem crossing processes, are also readily available.

Keywords: MLCT complexes; Quantum chemistry; Ultra-fast photodissociation; Wavepacket dynamics

1. Introduction

By the late seventies Dick Stufkens was already motivated by the assignment of the lowest energy absorption bands of transition metal α-diimine complexes and their role in the observed photophysics/photochemistry [1–3]. Since that time he gave this problem no peace using the most sophisticated spectroscopic techniques [4,5] until he answered these two fundamental questions:

i) Are the low-lying metal-to-ligand-charge-transfer states (MLCT) responsible for the low energy emission or electron/energy transfer processes directly involved in the observed photoreactivity?
ii) What is the role of the so-called sigma-bond-to-ligand-charge-transfer (SBLCT) state in the photoreactivity of this class of molecules?

In particular the photoreactivity of several RML(CO)x(α-diimine) (R = metal fragment, alkyl) complexes following irradiation into the visible energy domain (around 500 nm) characterized either by an heteroligand dissociation (most of the time CO loss) or by the homolytic cleavage of a metal–metal or metal–alkyl bond has puzzled the Amsterdam group for many

* Tel.: +33-390-241302; fax: +33-390-241589
E-mail address: daniel@quantix.u-strasbg.fr (C. Daniel).

0010-8545/02/$ - see front matter
PII: S0010-8545(02)00019-X

years. The very intense experimental activity developed by this group never prevented these experts in spectroscopy and photochemistry from watching the latest theoretical developments. Already in the early eighties, Alain Veillard was contacted by Dick Stufkens who wrote him a formal letter concerning the photoactive state of $Mn_2(CO)_{10}$.

Obviously at that time quantum chemical investigations of the excited states properties of large molecules were beyond the computational capabilities. Qualitative one-electron orbital energy diagrams built on the basis of Extended Hückel calculations and photoelectron spectra were the only available theoretical tools. The theoretical interpretations of absorption spectra and photochemical reactions were based on a simple analysis in terms of bonding and antibonding orbitals with some luck. Excitations to antibonding or from bonding orbitals with respect to a given chemical bond were supposed to lead to the breaking of this bond, resonance Raman spectra providing evidence of the main structural deformations in the excited states. When competitive primary reactions were observed either at a given irradiation wavelength or at different wavelengths a simple analysis based on the bonds strengths was performed.

The semi-empirical methods (INDO, CNDO, ZINDO) very successful at describing the low-lying excited states properties of organic molecules [6] were not systematically parameterized for inorganic compounds due to the lack of accurate experimental data. The ligand electrochemical parameter theory applied to the spectroscopy of ruthenium compounds with specific ligands is one example of the use of ZINDO for transition metal complexes [7–9]. In the mid-eighties new theoretical formalisms took into account the electronic correlation effects including a multi-configurational scheme of the wavefunctions. The Configuration Interaction (CI), Multi-Configuration -SCF (MC-SCF) or Complete-Active-Space-SCF (CASSCF) methods enabled the description of electronic excited states in transition metal complexes with a reasonable accuracy (0.25 eV) [10,11]. At the same time, progress made in Density Functional Theory (DFT) encouraged the application of this efficient method to transition metal complexes and in a number of cases to excited state calculations [12–14] with more or less success depending on the symmetry of the molecule and on the degree of purity of the excited states. A recent promising development of the DFT method, the so-called Time-Dependent-DFT based on linear response theory and taking care of the single excitations has lead to reliable assignment of the lower part of the absorption spectra of a number of transition metal complexes [15–17].

The high density of various excited states (MLCT, MC (metal-centered), SBLCT, intra-ligand (IL), ligand-to-ligand-charge-transfer (LLCT) in a limited domain of energy (UV–vis) makes the theoretical investigation of the absorption spectra of transition metal charge transfer complexes a challenge. Moreover, the occurrence of state mixing adds computational difficulties especially during the investigation of photochemical reactions when the character of the potential energy surfaces (PES) associated with the different excited states change drastically as a function of the nuclear coordinates. From this point of view the complexes investigated in Amsterdam are not really friendly with theoreticians. Indeed, most of the time the presence of low-lying unreactive MLCT states interacting with reactive MC or SBLCT states along some reaction coordinates explains the photochemical richness of these molecules under visible irradiation (Scheme 1).

The present contribution devoted to the retirement of Dick Stufkens will illustrate through a few significant examples the progress made in the last 20 years in the quantum chemical description of excited states in α-diimine transition metal complexes inspired by the Amsterdam group. The MLCT photoreactivity will be illustrated through the photodissociation dynamics of $(H)Mn(CO)_3(H–DAB)$ (DAB = 1,4-diaza-1,3-butadiene), model system for a series of $(R)Mn(CO)_3$(α-diimine) complexes (R = alkyl, benzyl, metal fragment, α-diimine = ^{i}Pr-DAB, ^{t}Bu-DAB, bpy, ^{i}Pr-PyCa), whereas the SBLCT photoreactivity will be illustrated for the rhenium analogue $(H)Re(CO)_3(H–DAB)$. The theoretical results obtained for a series of versatile [Ru(E)(E′)$(CO)_2$(α-diimine)] complexes illustrate the role of the ^{3}SBLCT state in radical formation.

2. Computational methods

The computational strategy used to describe the photophysics and photochemistry of MLCT complexes in the past five years is summarized below. A detailed description can be found in the original papers [18–20].

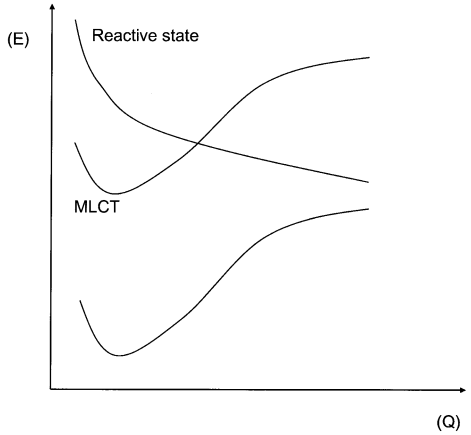

Scheme 1.

2.1. Excited states

Three methods of choice are actually available for the calculation of transition energies in middle sized (20–30 atoms) transition metal complexes:

i) The totally variational method based on an averaged CASSCF wavefunction describing the low-lying excited states of a given symmetry (five to ten eigenfunctions) supplemented by a Multi-Reference CI.
ii) A pertubational treatment of the dynamical correlation effects using the Second Order perturbation theory in the multi-state scheme so–called MS-CASPT2 on the top of a zero-order CASSCF wavefunction.
iii) A density functional approach based on the TD-DFT method.

The quality of the CASSCF wavefunction is given by the number of correlated electrons and the number and nature of orbitals included in the active space. The wavefunction has to be able to describe in a balanced way the electronic ground state as well as the different excited states (singlet and triplet of various symmetries) localized on the metal centre, on the ligands or of charge transfer types. The MR-CI method may compensate for the deficiency of restricted CASSCF active spaces whereas the use of perturbation theory (MS-CASPT2) should be restricted to cases where the zero-order CASSCF wavefunction describes correctly not only the non-dynamical correlation effects but also all the electronic states of interest. Otherwise serious intruder states problems will generate erroneous results. The limiting step is the CASSCF calculation which is time consuming and which cannot handle more than 16 electrons in the same numbers of active orbitals (in favorable situations of symmetric molecules). The CASSCF/MS-CASPT2 approach leads to satisfactory accuracy, most of the time better than 1500 cm^{-1}, whereas the CASSC/MR-CI method may overestimate the transition energies by more than 2000 cm^{-1} due to a limited description of the dynamical correlation effects with the MR-CI. An alternative to these sophisticated and expensive methods is the TD-DFT approach, which is very efficient for the computation of the lowest excited states and associated oscillator strengths. However, this method is based on the electronic ground state density and the one-electron excitations are performed on the basis of the corresponding Kohn–Sham orbitals, the electronic relaxation in the excited states being neglected. As a consequence when the electronic ground state density is a good approximation to the excited state density this latter will be correctly described otherwise erratic results will be obtained and the interpretation will become problematic [17,21].

2.2. Potential energy surfaces

Computation of the potential energy curves and surfaces associated with the electronic excited states is even more difficult. Until now, applications to transition metal complexes have been restricted to two-dimensional potential energy surfaces (PES), the highest symmetry being retained along the reaction pathways. A limited evaluation of the geometrical relaxation effects in the electronic excited states is performed. The molecule is frozen in its Franck–Condon electronic ground state structure, known either from X-ray experiments or from DFT optimizations. The potential energy curves (surfaces) are calculated as a function of the reaction coordinate (coordinates) describing the primary reaction (reactions) observed after irradiation of the molecule. It is supposed that the elementary events leading to the primary products (radicals, unsaturated species) are extremely fast (femtosecond-picosecond time scale).

Obviously the CASSCF wavefunction has to describe correctly the reactant in the Franck–Condon region (excited states) as well as the bonding changes along the reaction coordinate and the primary products. In particular, the change of character of an electronic state as a function of the reaction coordinate (avoided crossings) has to be taken into account. Usually the CASSCF/MR-CI method is more reliable than the perturbation theory for such problems even though it is less accurate than the CASSCF/MS-CASPT2. The use of TD-DFT method for the computation of potential energy curves has to be performed with care [21].

2.3. Excited states dynamics

The excited states dynamics are followed by wavepacket propagations on the potential energy curves (surfaces). A wavepacket is a coherent superposition of stationary states. In order to simulate the absorption, the initial wavepacket is built on the basis of the vibrational ground state of the electronic ground state. When multiplied by the transition dipole moment the absorbing state will be populated (Scheme 2).

Since the wavepacket is not an eigenfunction of the excited electronic state it will evolve as a function of time on the excited potential. This evolution can be followed by solving the time-dependent Schrödinger equation. The time evolution can be followed either on a single potential (for instance the absorbing state in the visible) or on several potentials coupled by spin-orbit and non-adiabatically (avoided crossings). Several quantities may be extracted from these simulations [18,19,22]:

i) The autocorrelation function which gives the overlap between the wavepacket at time $t = 0$ and time t.

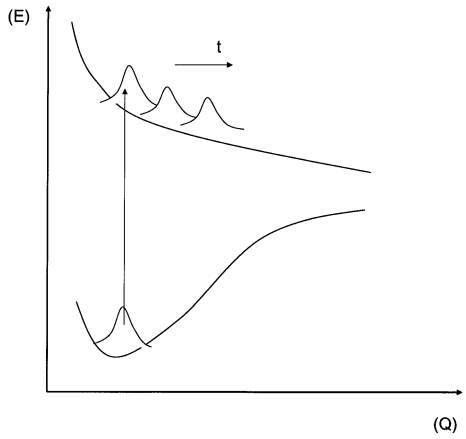

Scheme 2.

ii) The absorption spectrum, Fourier transform of the autocorrelation function.
iii) The population of the different potentials as a function of time.
iv) The probability of dissociation.
v) The time scales for elementary processes such as direct dissociation, intersystem crossing, internal conversion.
vi) The branching ratio between competitive channels.

The main features of the absorption spectrum, the primary products distribution validate a posteriori the simulation which is reliable only for events occurring in the first ps. Indeed, in a longer time-scale other competitive elementary processes (emission) or relaxation effects (deformation along other degrees of freedom) may operate.

3. An example of a reactive MLCT state: photodissociation dynamics of (H)Mn(CO)$_3$(H–DAB)

The electronic spectroscopy and photodissociation dynamics of (H)Mn(CO)$_3$(H-DAB) (DAB = 1,4-diaza-1,3-butadiene) [19] (Fig. 1), a model for a series of (R)Mn(CO)$_3$(α-diimine) complexes studied in Amsterdam, give a beautiful illustration of the role of the MLCT states in the photoreactivity of these molecules.

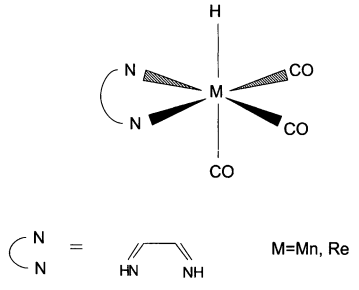

Fig. 1. Idealized molecular structute of (H)M(CO)$_3$(H–DAB) (M = Mn, Re).

According to a number of experiments reported for a series of (R)Mn(CO)$_3$(α-diimine) complexes [5,23–25] these molecules may adopt different photochemical behavior under irradiation at 500 nm leading either to CO loss or to the homolysis of the Mn–R bond the quantum yields depending on the nature of R,

$$(R)Mn(CO)_3(\alpha\text{-diimine}) \xrightarrow{h\nu} CO + (R)Mn(CO)_2 \times (\alpha\text{-diimine}) \quad (1)$$

$$(R)Mn(CO)_3(\alpha\text{-diimine}) \xrightarrow{h\nu} R^{\bullet} + {}^{\bullet}Mn(CO)_3 \times (\alpha\text{-diimine}) \quad (2)$$

The aim of the theoretical study was to understand the mechanism and search for the photoactive excited states responsible for the observed primary reactions (1) and (2).

On the basis of wavepacket propagations on the two-dimensional PESs (Fig. 2) calculated as a function of the q_a = [Mn–H] and q_b = [Mn–CO$_{ax}$] coordinates (Scheme 3) the following mechanism has been proposed (Fig. 3) [19]:

i) Irradiation in the visible will bring the system into the ^{1}MLCT ($3d_{xz} \rightarrow \pi^*_{DAB}$) absorbing state calculated at 23 000 cm^{-1} with an oscillator strength of 0.39.
ii) The dissociative character of the potential associated with this excited state as a function of the Mn–CO$_{ax}$ bond elongation makes direct dissociation to the primary products CO + (H)Mn(CO)$_2$(DAB) total and very efficient.

Non-radiative transitions to the low-lying triplet states and homolysis of the metal–H bond are not competitive with this total, direct and ultra-fast process which leads to CO loss products within 400 fs in the model system.

This mechanism explains the high quantum yields ($0.6 < \Phi_{CO} < 1.0$) observed for CO loss in this class of complexes [23,24]. The Mn–R bond homolysis in these complexes will occur through ^{1}MLCT → ^{3}SBLCT intersystem crossing, the ^{3}SBLCT state corresponding to the $\sigma_{Mn-R} \rightarrow \pi^*_{DAB}$ excitation. In the model system population of the ^{3}SBLCT state after one ps of simulation is negligible (less than 1%). This is due to weak spin orbit coupling between the ^{1}MLCT and ^{3}SBLCT states (75 cm^{-1}) associated with an unfavorable position of the singlet/triplet crossing in the Franck–Condon region. In the real systems the nature of the α-diimine and R groups (R = methyl, ethyl, benzyl) may influence this latter point leading to more efficient intersystem crossing and consequently to an increase in the quantum yield of the metal-bond homolysis.

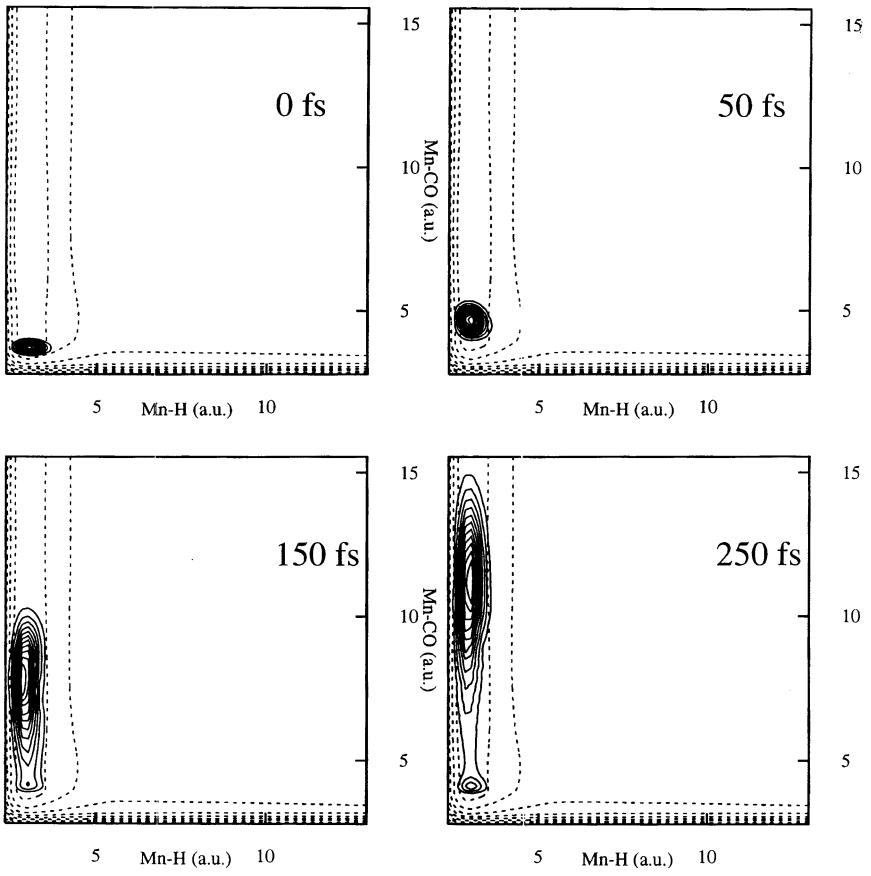

Fig. 2. Time evolution of a selected wavepacket (continuous line) on the 2-D (q_a = [Mn–H] and q_b = [Mn–CO_{ax}]) PESs (dotted line) associated with the absorbing ^{1}MLCT state of (H)M(CO)$_3$(H–DAB).

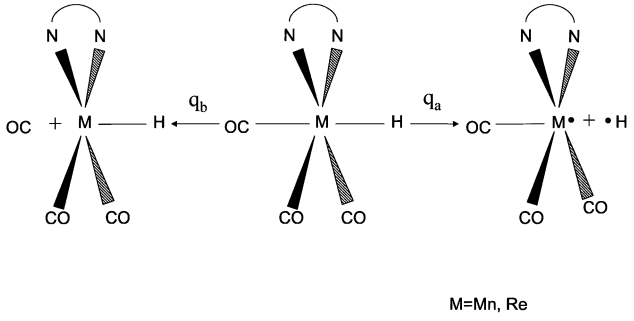

Scheme 3.

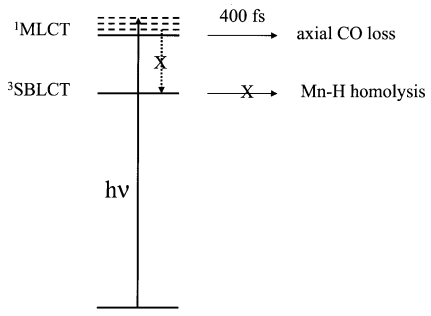

Fig. 3. Mechanism of photodissociation of (H)M(CO)$_3$(H–DAB) after irradiation into the visible.

Obviously the nature of the metal centre will drastically modify the photoreactivity as illustrated by the rhenium analogue in the next section.

4. The role of the ^{3}SBLCT state

The role of the ^{3}SBLCT state in the homolysis of metal–R bonds (R = alkyl, benzyl, halides, metal frag-

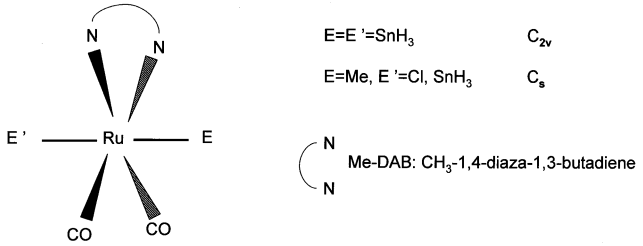

Fig. 4. Idealized molecular structure of the [Ru(E)(E′)(CO)$_2$(Me-DAB)] complexes.

ments) in a variety of α-diimine transition metal complexes is illustrated by two applications:

i) The photodissociation dynamics of (H)Re(CO)$_3$(DAB) (Fig. 1), model system for a series of (R) Re(CO)$_3$(α-diimine) complexes [26–28].
ii) The photoreactivity of [Ru(E)(E′)(CO)$_2$(Me-DAB)] systems (Fig. 4), models for the [Ru(E)(E′)(CO)$_2$(α-diimine)] (E,E′ = halide, alkyl, benzyl, metal-fragment;α-diimine = derivatives of 1,4-diaza-1,3-butadiene or 2,2′-bipyridine) complexes [29–32].

For the rhenium complex a complete quantum chemical study has been performed based on wavepacket simulations on two-dimensional PESs [33] whereas the results presented for the ruthenium compounds include preliminary simulation of the dynamics based on one-dimensional potential energy curves.

4.1. Photodissociation dynamics of (H)Re(CO)$_3$(H–DAB)

In contrast to the manganese analogue, the (R) Re(CO)$_3$(α-diimine) complexes undergo a unique major primary reaction after irradiation in the visible, namely the homolytic rupture of the Re–R bond.

$$(R)Re(CO)_3(\alpha\text{-diimine}) \xrightarrow{h\nu} R^{\bullet} + {}^{\bullet}Re(CO)_3 \times (\alpha\text{-diimine}) \quad (3)$$

The quantum yield Φ_{Re-R} may vary between 10^{-2} (R = methyl) to 1.0 (R = benzyl or ethyl) [26,27]. The alternative to the homolytic cleavage of the metal–R bond is an intense emission indicating the presence of a long lived triplet excited state precursors of electron/energy transfer processes.

On the basis of wavepacket propagations on the two-dimensional PESs calculated as a function of the q_a = [Re–H] and q_b = [Re–CO$_{ax}$] coordinates (Scheme 3) the following mechanism has been proposed (Fig. 5):

i) Irradiation in the visible will bring the molecule into the ^{1}MLCT ($5d_{xz} \rightarrow \pi^*_{DAB}$) absorbing state calculated at 22 500 cm^{-1} with an oscillator strength of 0.38.
ii) The system becomes trapped in the potential well of the absorbing state, which is bound for both channels namely, the CO loss and the metal–H bond homolysis.
iii) After a few tens of fs the low-lying ^{3}SBLCT state is preferably populated over the other triplet states through ^{1}MLCT → ^{3}SBLCT intersystem crossing.
iv) The homolytic cleavage of the Re–H bond occurs along the ^{3}SBLCT potential which is dissociative with respect to this bond elongation.

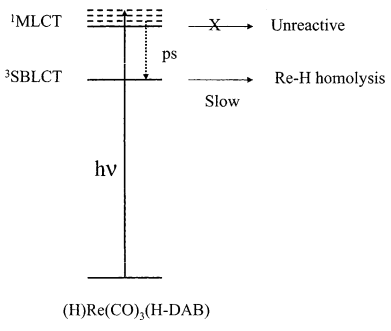

Fig. 5. Mechanism of photodissociation of (H)Re(CO)$_3$(H–DAB) after irradiation into the visible.

In contrast to the manganese analogue where the ^{1}MLCT → ^{3}SBLCT intersystem crossing is quenched by the efficient and ultra-fast CO loss due to the dissociative character of the absorbing state (Fig. 3) the rhenium compounds has a totally unreactive ^{1}MLCT state. As a consequence the intersystem crossing process becomes efficient. Moreover the spin-orbit coupling between the ^{1}MLCT and ^{3}SBLCT states in (H)Re(CO)$_3$(DAB) is larger than in the first-row transition metal complex (310 vs. 75 cm^{-1}). The photodissociation dynamics is controlled by the spin-orbit coupling between the two states and by the position of their crossing along the reactive channel. In agreement with the modest quantum yield characterizing the Re–Me bond homolysis in the methyl substituted complexes the probability of dissociation in the model system remains very low (2%) after three ps of simulation pointing to a non-total process. The proposed mechanism explains the wavelength and temperature dependence of the quantum yield in the series of rhenium complexes. Indeed, increasing the wavelength of irradiation or the temperature, the system gains some vibrational energy in the ^{1}MLCT absorbing state and by a simple dynamical effect the probability to reach the ^{1}MLCT/^{3}SBLCT crossing point will increase as well.

Aside from the spin-orbit coupling effect, which differs between the manganese and the rhenium complexes, the bonding interactions are slightly different and may explain the bound character of the ^{1}MLCT absorbing state in the third-row transition metal complex. In (H)Mn(CO)$_3$(DAB) the predominant interactions between the metal centre and the carbonyls are the dπ–pπ back bonding interactions (Scheme 4).

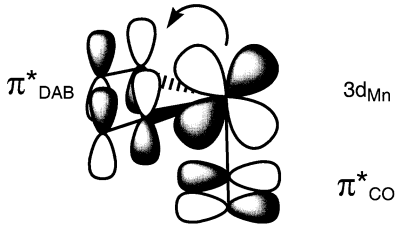

Scheme 4.

When exciting one electron from the $3d_{xz}$ orbital to the π^*_{DAB} orbital this stabilizing interaction with the axial CO ligand decreases with a weakening of the Mn–CO_{ax} bond. In contrast the main stabilizing interaction between the rhenium atom and the axial CO ligand is based on the p diffuse orbital of the rhenium. Consequently, depopulation of the $5d_{xz}$ orbital will have little influence on the metal–CO_{ax} bonding and the potential associated to the ^{1}MLCT state will remain bound.

4.2. Photoreactivity of a series of *[Ru(E)(E′)(CO)$_2$(Me-DAB)] complexes*

A series of versatile transition metal carbonyl–diimine complexes [Ru(E)(E′)(CO)$_2$(α-diimine)] (E,E′ = halide, alkyl, benzyl, metal-fragment;α-diimine = derivatives of 1,4-diaza-1,3-butadiene or 2,2′-bipyridine) has been investigated in Amsterdam for their unconventional photochemical, photophysical and electrochemical properties. In the series or even within the same molecule, several different types of charge transfer transitions from the metal, the halide ligand or from the axial σ bond to the σ acceptor α-diimine group coexist leading to important spectroscopic and photochemical consequences [29–32].

Two classes of compounds have been studied, namely the halide and the non-halide substituted molecules characterized by contrasting spectroscopic and photochemical properties. The halides display a strong solvatochromic absorption between 400–450 nm assigned either to MLCT or XLCT transitions. A large stokes shift points to an important distortion in the emitting excited states, which has a rather, long life-time (up to a few tens of ns). The emission is observed between 630–650 nm with a time-scale of a few tens of μs and modest quantum yields ($\Phi_{em} \approx 10^{-4}$). Important resonance Raman effects point to electronically localized systems. The halide substituted molecules are unreactive at low temperature as well as at room temperature. In contrast the non-halide systems are photolabile under irradiation in the visible at room temperature leading to radical primary products with modest quantum yields ($0.006 < \Phi < 0.3$).

$$[\mathrm{Ru(E)}(E')(\mathrm{CO})_2(\alpha\text{-diimine})] \xrightarrow{h\nu} \mathrm{E}^{\bullet} + {}^{\bullet}\mathrm{Ru}(E')(\mathrm{CO})_2 \times (\alpha\text{-diimine}) \quad (4)$$

The homolytic cleavage of the Ru–E bond is rather slow (ps to ns), wavelength independent but temperature dependent. Most of the time this process is selective with respect to the Ru–E and Ru–E′ bonds. The non-halides present an absorption around 500 nm with a weak solvatochromism assigned to SBLCT transitions. The distortion in the excited state is rather small with a unusually long life-time (0.5 to 36 μs). An emission is observed between 550 and 670 nm with a rather long life-time (up to 260 μs) and a modest quantum yield ($0.001 < \Phi_{em} < 0.015$).

These spectroscopic and photochemical features are a big challenge to the interplay between theory and experiment and have important implications for the photochemistry and spectroscopy of low-valent metal complexes simultaneously containing electron-accepting ligands and π-donors such as halides and/or σ-bonded alkyl or metal fragments.

In order to rationalize the behavior of this series of complexes after irradiation in the visible quantum chemical calculations have been performed for the [Ru(SnH$_3$)$_2$(CO)$_2$(Me-DAB)], [Ru(Me)(SnH$_3$)(CO)$_2$-(Me-DAB)] and [Ru(Me)(Cl)(CO)$_2$(Me-DAB)] complexes (Fig. 4), model systems for [Ru(E)(E′)(CO)$_2$(^{i}Pr-DAB)] (E = E′ = SnPh$_3$; E = SnPh$_3$ or Cl, E′ = Methyl; ^{i}Pr-DAB = *N*,*N*′-di-isopropyl-1,4-diaza-1,3-butadiene).

The low-lying excited states and associated potential energy curves as a function of the Ru–E bond elongation (Ru–SnH$_3$, Ru-Me) (Scheme 5) have been calculated at the CASSCF/MS-CASPT2 level of theory.

4.2.1. The non-halides complexes: *[Ru(SnH$_3$)$_2$(CO)$_2$(Me-DAB)] and [Ru(Me)(SnH$_3$)(CO)$_2$(Me-DAB)]*

The visible bands of these complexes which possess very similar absorption spectra [17] with one band centered around 19 000 cm^{-1} are mainly composed of the ^{1}SBLCT transition corresponding to the $\sigma_{ERuE'} \rightarrow \pi^*_{DAB}$ excitation (E = E′ = SnH$_3$ or E = Me, E′ = SnH$_3$, σ being the anti symmetrical bonding orbital between the 5p(Ru) and the sp3-like orbitals of the axial ligands E and E′). This transition is calculated at 21 260 and 20 400 cm^{-1} for the [Ru(SnH$_3$)$_2$(CO)$_2$(Me-DAB)] and [Ru(Me)(SnH$_3$)(CO)$_2$(Me-DAB)] complexes, respectively, with oscillator strengths of 0.17 and 0.11. The MLCT states are predicted in the UV/near-UV energy domain with strong absorptions at 29 220 and 25 690 cm^{-1} for the Sn–Sn and Sn–Me substituted molecules, respectively.

In order to follow the photoreactivity of these two model systems and to understand the photolability of the [Ru(SnPh$_3$)$_2$(CO)$_2$(^{i}Pr-DAB)] and [Ru(SnPh$_3$)(Me)-(CO)$_2$(^{i}Pr-DAB)] complexes at room temperature the CASSCF/CASPT2 potential energy curves associated

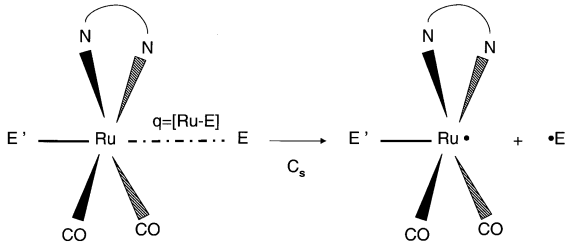

Scheme 5.

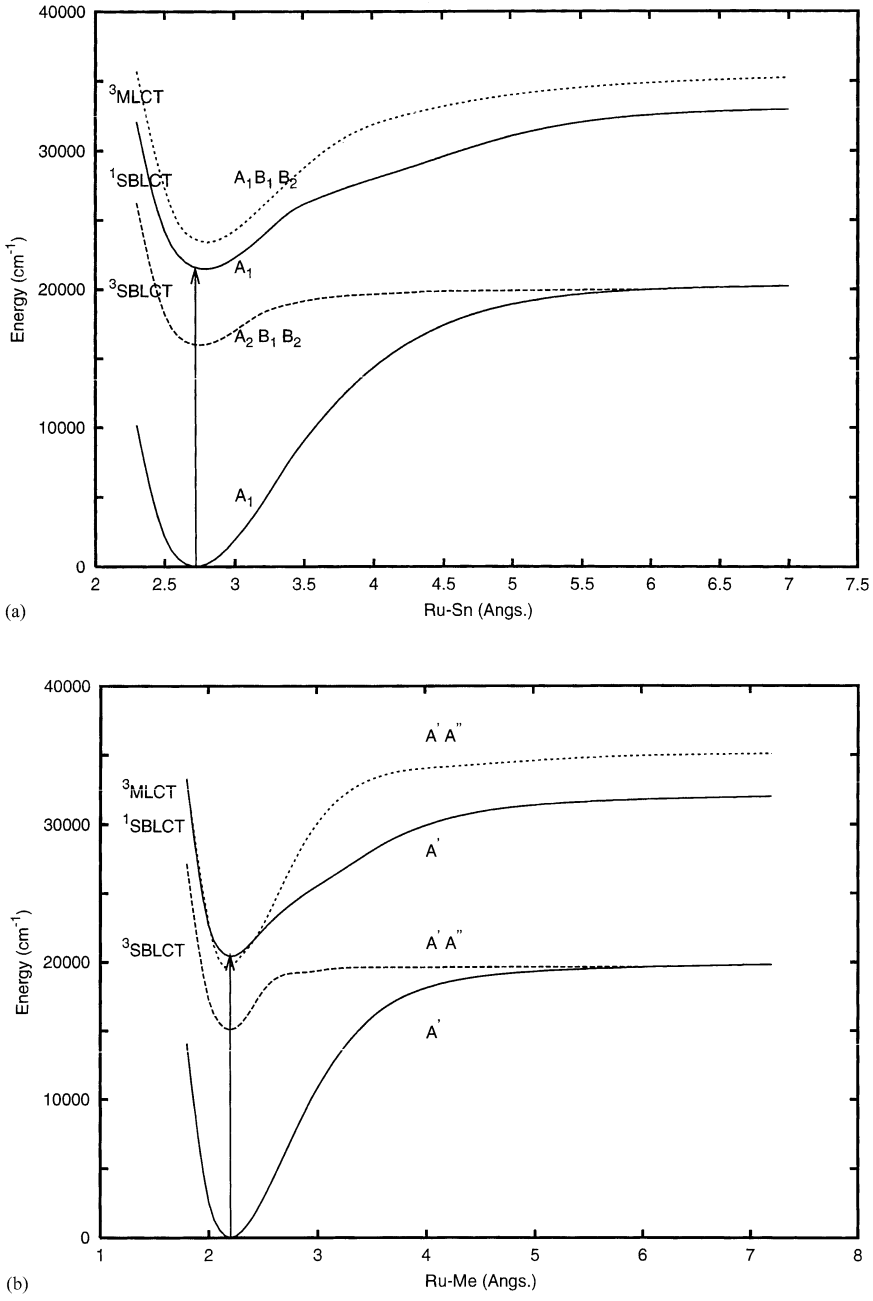

Fig. 6. CASSCF/MS-CASPT2 potential energy curves of (a) $[Ru(SnH_3)_2(CO)_2(Me\text{-}DAB)]$ as a function of the Ru–Sn bond elongation (b) $[Ru(SnH_3)(Me)(CO)_2(Me\text{-}DAB)]$ as a function of the Ru–Me bond elongation

with the ^{1}SBLCT absorbing state and low-lying ^{3}SBLCT and ^{3}MLCT states have been calculated as a function of the Ru–Sn and Ru–Me bond elongations under C_{2v} and C_s symmetry constraints, respectively (Fig. 6(a and b)). Even though the absorption spectra of the two systems are very similar, their photoreactivity differs significantly [30]. According to the experiments, the photochemical homolysis of the Ru–Sn bond observed at room temperature in $[Ru(SnPh_3)_2(CO)_2(^i Pr\text{-}DAB)]$ with a quantum yield of 0.23 and which is supposed to occur through the ^{3}SBLCT state is rather slow due to a thermally activated mechanism. Moreover, the ^{3}SBLCT, despite its reactivity is very stable with a lifetime of 1 μs.

In contrast, the Ru–Me bond homolysis in $[Ru(SnPh_3)(Me)(CO)_2(^i Pr\text{-}DAB)]$ occurs very rapidly, the radical formation in THF solutions being fully completed within the 10 ns excitation pulse.

The shape of the potential energy curves associated with the ^{1}SBLCT and ^{3}SBLCT states are very similar in both complexes (Fig. 6(a and b)) and cannot explain the significant different reactivities. The absorbing state is bound with respect to homolysis and the ^{3}SBLCT state

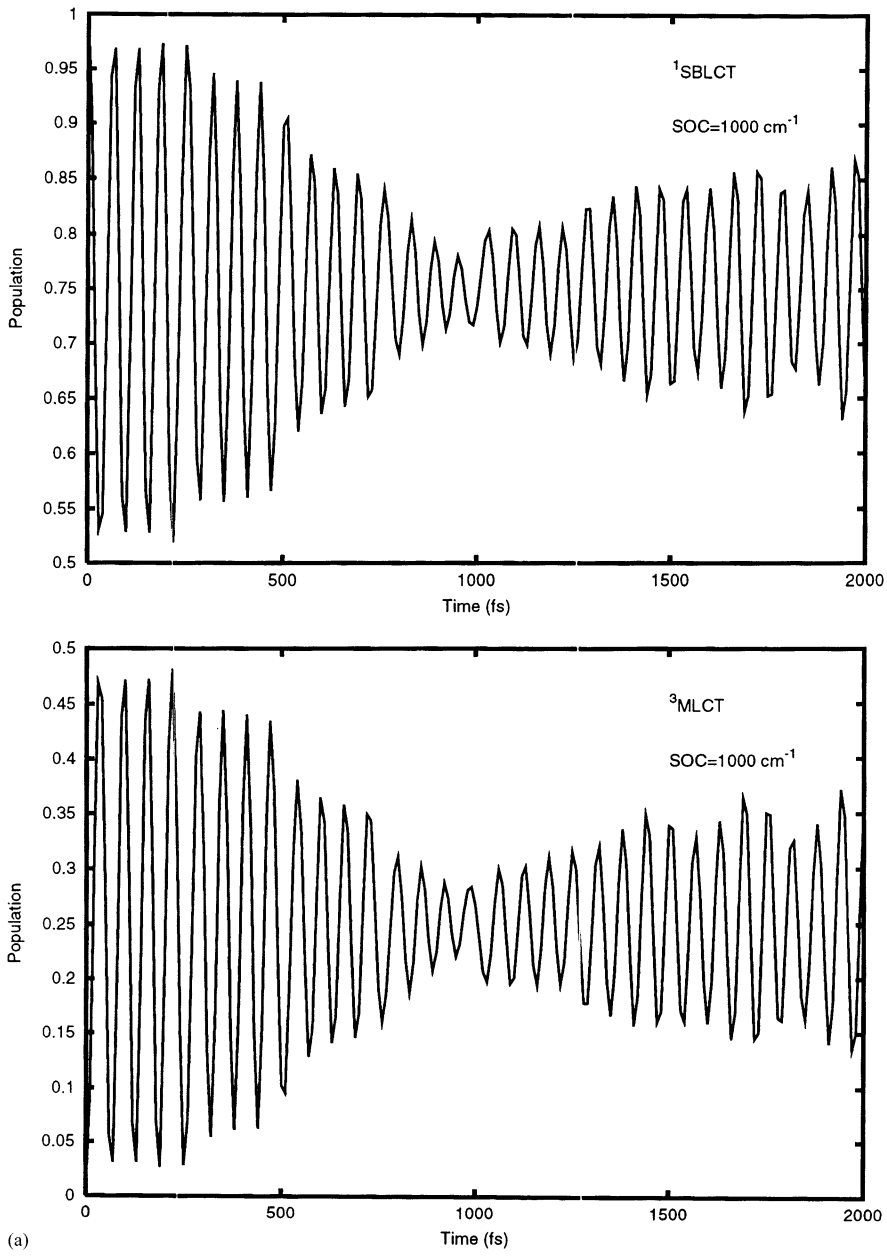

Fig. 7. Time evolution of the population of the ^{1}SBLCT absorbing state and of the low-lying triplet states of (a) [Ru(SnH$_3$)$_2$(CO)$_2$(Me-DAB)] and (b) [Ru(SnH$_3$)(Me)(CO)$_2$(Me-DAB)] accessible through first-order intersystem crossing.

which correlates with the radical primary products of the homolysis own a potential well in both complexes.

However, a qualitative estimation of the spin-orbit interactions in the two model systems point to quite large differences in the ^{1}SBLCT → ^{3}SBLCT intersystem crossing mechanism. As illustrated in Fig. 6(a) [Ru(SnH$_3$)$_2$(CO)$_2$(Me-DAB)] the ^{3}SBLCT state belonging to the A_1 symmetry will be split into three A_2, B_1 and B_2 components by spin-orbit whereas the ^{3}MLCT state of A_2 symmetry will be split into A_1, B_1 and B_2 components. As a consequence, the SO interaction between the ^{1}SBLCT state and the ^{3}SBLCT state leading to the homolytic splitting will operate in second order. The ^{1}SBLCT → ^{3}SBLCT intersystem crossing will be characterized by low efficiency in contrast to the ^{1}MLCT → ^{3}MLCT intersystem crossing process.

Under experimental conditions a small distortion of the molecule by temperature or environment effects could activate the ^{1}SBLCT → ^{3}SBLCT intersystem crossing and initiate the homolytic cleavage of the Ru–Sn bond along the ^{3}SBLCT potential energy curve in a slow and non-total process.

In the [Ru(Me)(SnH$_3$)(CO)$_2$(Me-DAB)] of low symmetry (C_s) both the ^{1}SBLCT → ^{3}SBLCT and

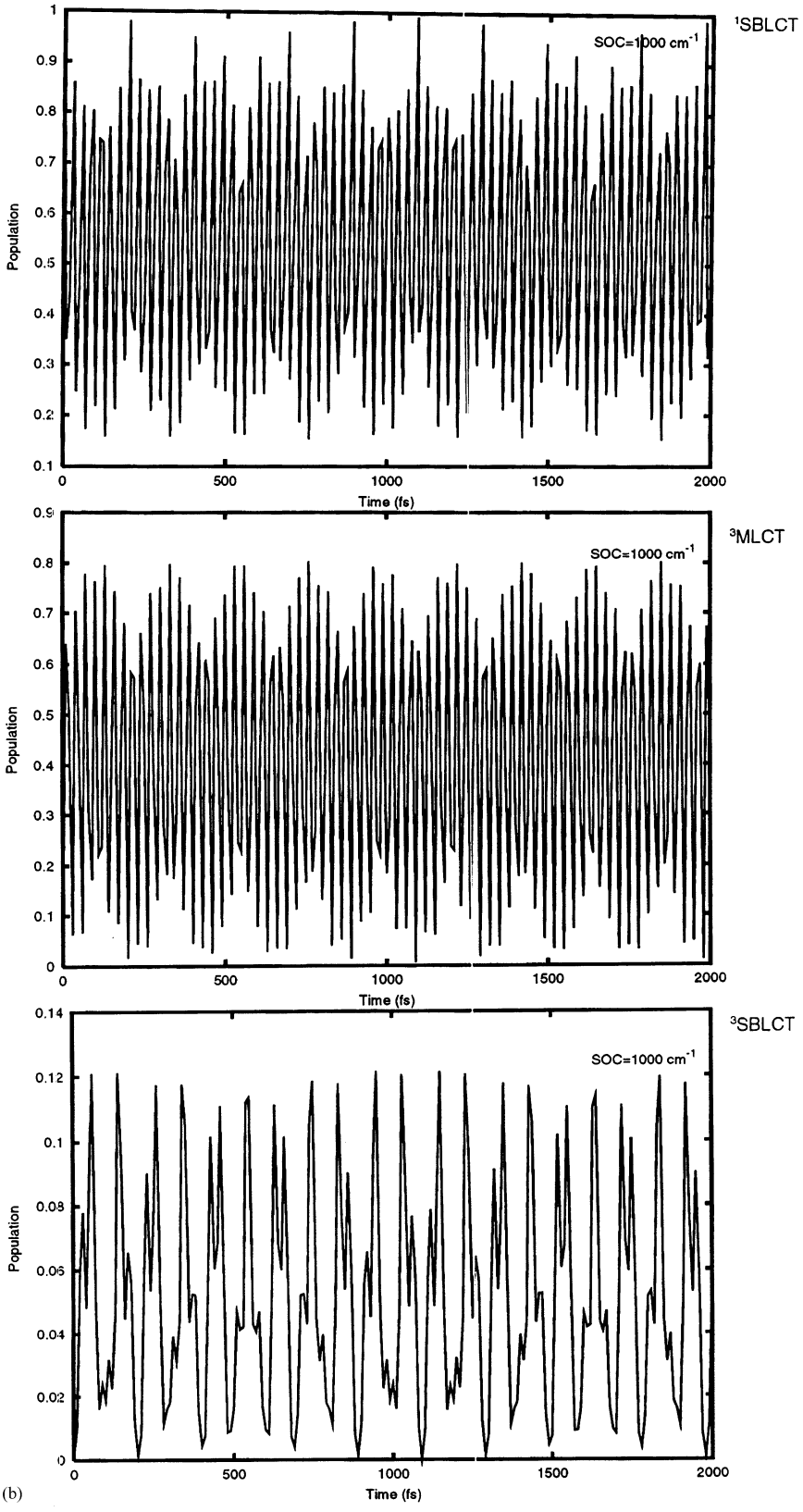

(b)

Fig. 7 (*Continued*)

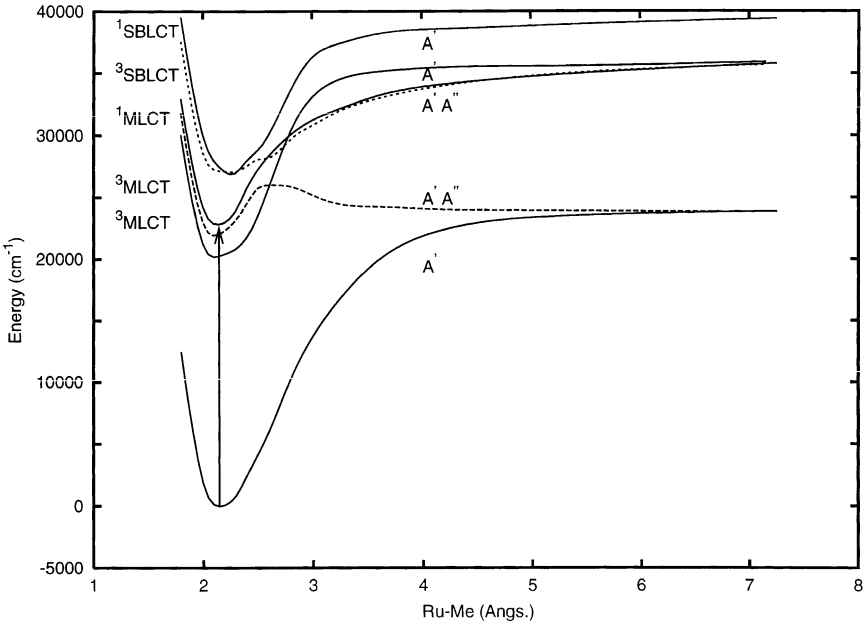

Fig. 8. CASSCF/MS-CASPT2 potential energy curves of [Ru(Me)(Cl)$(CO)_2$(Me-DAB)] as a function of the Ru–Me bond elongation.

^{1}MLCT → ^{3}MLCT intersystem crossings are efficient in the Franck–Condon region, both triplets having a A′ component by spin-orbit splitting able to interact in first order with the ^{1}SBLCT absorbing state of A′ symmetry (Fig. 6(b)).

In order to illustrate the different behavior with respect to spin-orbit coupling effects, preliminary wave-packet dynamics have been performed on the spin-orbit coupled potentials depicted in Fig. 6(a and b) for a spin-orbit interaction estimated at 1000 cm^{-1}. For the [Ru$(SnH_3)_2(CO)_2$(Me-DAB)], only the ^{1}SBLCT/^{3}MLCT spin-orbit coupling (first-order interaction) has been turned on in the time-dependent Schrödinger equations, whereas in [Ru(Me)$(SnH_3)(CO)_2$(Me-DAB)] the ^{1}SBLCT/^{3}SBLCT and ^{1}SBLCT/^{3}MLCT spin-orbit have been turned on. The populations of the different excited states has been followed as a function of time between zero fs and two ps (Fig. 7(a and b)).

In the limit of this simulation within two ps restricted to one dimension (either the Ru–Sn or the Ru–Me bond elongation) the main elementary event in the Sn–Sn substituted complex is the population of the ^{3}MLCT (45% in a few tens of fs) (Fig. 7(a)). In the Sn–Me substituted complex both the ^{3}SBLCT and ^{3}MLCT states are populated immediately after irradiation in the visible energy domain (Fig. 7(b)). Due to the energy gap the ^{1}SBLCT → ^{3}SBLCT intersystem crossing seems to be less efficient than the ^{1}SBLCT → ^{3}MLCT intersystem crossing as illustrated by the time evolution of the population of the three states. The population of the ^{3}MLCT state, which is nearly degenerate with the absorbing state in the Franck–Condon region reaches 80% in the first tens of fs whereas only 12% contributes to the ^{3}SBLCT population within the same time.

4.2.2. *The halides complexes: [Ru(Me)(Cl)$(CO)_2$(Me-DAB)]*

In contrast to the non-halide complexes the visible band of the absorption spectrum of the chloride substituted complex centered around 21 000 cm^{-1} [17] corresponds mainly to MLCT transitions with a strong absorption calculated at 22 630 cm^{-1} in the model complex with an oscillator strength of 0.23. The ^{1}SBLCT state calculated at 26 830 cm^{-1} and corresponding to the $\sigma_{Me-Ru} \rightarrow \pi^*_{DAB}$ excitation is predicted in the UV energy domain.

The CASSCF/MS-CASPT2 potential energy curves calculated as a function of the Ru–Me bond elongation under a C_s symmetry constraint are reported for the ^{1}MLCT, ^{1}SBLCT and low-lying triplet states in Fig. 8.

The photodissociation of the model complex is characterized by two sets of avoided crossings between the absorbing ^{1}MLCT state and the upper ^{1}SBLCT state and between the corresponding triplet states as a function of the homolysis coordinate. The character of the ^{1}MLCT and ^{3}MLCT states will change drastically along the reaction pathway, their SBLCT nature increasing as a function of the Ru–Me bond distance. After irradiation in the visible the system becomes trapped in the potential wells of the ^{1}MLCT state and of the two low-lying triplet states as illustrated by the time evolution of the population of the three states (Fig. 9).

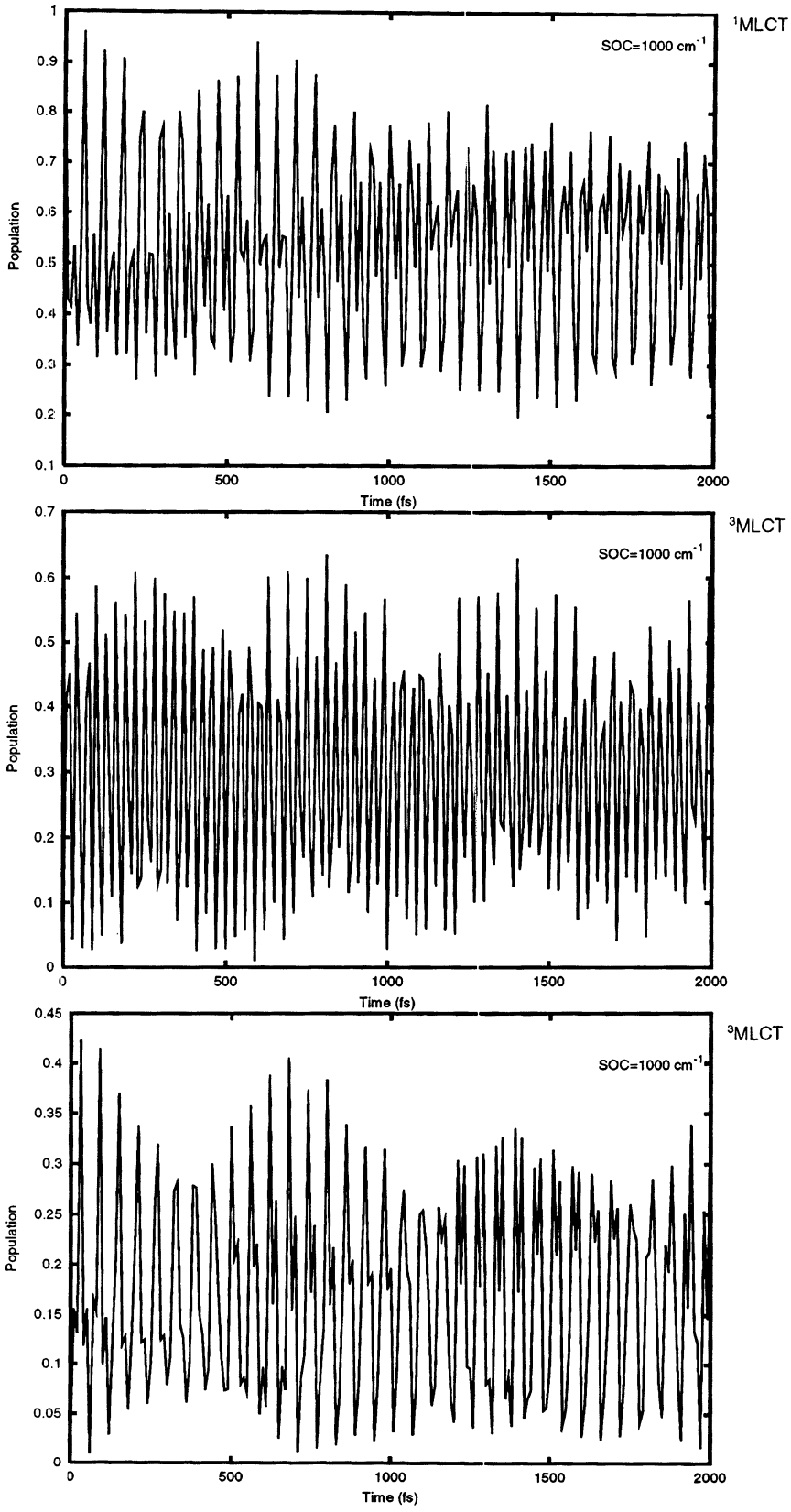

Fig. 9. Time evolution of the populations of the ^{1}SBLCT absorbing state and of the low-lying triplet sates of [Ru(Me)(Cl)$(CO)_2$(Me-DAB)] accessible through first order intersystem crossing.

In the limit of this one dimensional simulation performed within 2 ps the populations of the low-lying ^{3}MLCT states reach 60 and 42% in less than 100 fs.

Clearly the dissociative pathway towards the radical primary products is unlikely due to the presence of an energy barrier ($\sim$4000 cm^{-1}) along the ^{3}MLCT potential energy curve (before 3.0 Å) generated by the ^{3}SBLCT/^{3}MLCT avoided crossing. Quenching by efficient trapping into the MLCT potentials wells will lead to emissive processes.

5. Conclusion

The collaboration maintained with the Amsterdam group over nearly 15 years is a beautiful example of interplay between experiment and theory. A few students from Amsterdam came to Strasbourg during their Ph.D. studies for experimenting with computational methods. One student in Quantum Chemistry spent a period in Amsterdam to collect her own absorption spectrum for comparison with the results of the simulation. Even if only a few joint papers were published, the number of informal exchanges and discussions about fascinating and fundamental questions kept our cooperation active through two successive European COST actions.

Obviously, the task of the theoreticians as far as the spectroscopy and photochemistry of large MLCT complexes are concerned is still enormous. One of the main difficulties is to find reliable model systems able to describe correctly the properties of the real systems investigated experimentally. The experimentalists can vary the surrounding ligands, metal centre and the experimental conditions with a reasonable frequency on a time scale of one Ph.D. thesis. In contrast the theoreticians have to invest so much time in the 'preliminary' calculations that they cannot follow these changes.

Despite these difficulties, it has been possible to extract general trends from this fruitful interplay between experiment and theory discussed in detail in a number of articles devoted to the theoretical study of MLCT photochemistry [19,20,33,34]. The high photoreactivity of first-row transition metal α-diimine complexes after irradiation in the visible region observed in a number of chromium and manganese complexes can be explained on the basis of the results reported for the model system (H)(Mn(CO)$_3$(H–DAB). Namely, efficient CO loss due to the repulsive character of the potential associated with the ^{1}MLCT absorbing state quenches the elementary processes towards other deactivation channels. This is due to the weakening of the metal–CO$_{axial}$ bond by excitation from the metal centre to the low-lying π* acceptor α-diimine ligand. This effect is less important in third-row transition metal complexes due to different metal–CO bonding interactions. Consequently the photophysics of third-row coordination compounds is often more rich than the first-row analogue. The key role of the so-called ^{3}SBLCT state in the formation of diradical primary products discussed in the model systems (H)(Re(CO)$_3$(H–DAB) or [Ru(E)(E′)(CO)$_2$(Me-DAB)] can be extended to a variety of α-diimine complexes for which metal–alkyl or metal–metal bond breaking have been observed upon visible light irradiation. In contrast with a common naive picture based on molecular orbital (MO) theory valid for ground states properties only there is no direct correlation between the bonding–antibonding character of the MOs populated by excitation and the observed photochemistry. In the same way the relative bond strengths do not control the outcome of the photoinduced reactions.

Future work will probably evolve to develop methods able to provide multi-dimensional PESs. An alternative is the determination of crucial critical geometries along these PESs, which drive the dynamical processes, as has been done in organic photochemistry [35]. In order to approach the real experiments the environmental effects will have to be taken into account. The development of femtosecond lasers and their use in coordination chemistry has contributed to the building of an important bridge between theoreticians and experimentalists and brings some hope for future fruitful collaborations.

Acknowledgements

The author is grateful to Professor Dick Stufkens for his interest and his motivation in the quantum chemical description of excited states properties. Three theses were undertaken in quantum chemistry in Strasbourg on complexes from Amsterdam motivated by the continual questions of Professor Dick Stufkens on a variety of fascinating problems. The author thanks Dominique Guillaumont who was a pioneer in the field of MLCT photochemistry, Isabelle Bruand-Cote and Mohamed Turki for their work on the rhenium and ruthenium complexes. This work has been undertaken as part of the European collaborative COST project (D14/0001/99).

References

[1] R.W. Balk, D.J. Stufkens, A. Oskam, Inorg. Chim. Acta 28 (1978) 133.
[2] L.H. Staal, D.J. Stufkens, A. Oskam, Inorg. Chim. Acta 26 (1978) 255.
[3] R.W. Balk, D.J. Stufkens, A. Oskam, Inorg. Chim. Acta 34 (1979) 267.
[4] D.J. Stufkens, Coord. Chem. Rev. 104 (1990) 39.
[5] D.J. Stufkens, Comments Inorg. Chem. 13 (1992) 359.

[6] U. Dimur, M. Karplus, Chem. Phys. Lett. 88 (1982) 171.
[7] S.I. Gorelsky, E.S. Dodsworth, A.B.P. Lever, A. Vlcek, Jr., Coord. Chem. Rev. 174 (1998) 469.
[8] C.J. da Cunha, E.S. Dodsworth, M.A. Monteiro, A.B.P. Lever, Inorg. Chem. 38 (1999) 5399.
[9] M. Nazuruddin, S.M. Zakeeruddin, R. Humphry-Baker, S.I. Gorelsky, A.B.P. Lever, M. Grätzel, Coord. Chem. Rev. 208 (2000) 213.
[10] C. Daniel, T. Matsubara, G.J. Stor, Coord. Chem. Rev. 132 (1994) 63.
[11] D. Guillaumont, C. Daniel, A. Vlcek, Jr., Inorg. Chem. 36 (1997) 1684.
[12] P.C. Servaas, D.J. Stufkens, A. Oskam, P. Vernooijs, E.J. Baerends, D.J.A. DeRidder, C.H. Stam, Inorg. Chem. 28 (1989) 4104.
[13] C. Daul, E.J. Baerends, P. Vernooijs, Inorg. Chem. 33 (1994) 3538.
[14] G.J. Stor, D.J. Stufkens, P. Vernooijs, E.J. Baerends, J. Fraanje, K. Goubitz, Inorg. Chem. 34 (1995) 1588.
[15] S.I. Gorelsky, S. da Silva, A.B.P. Lever, D.W. Franco, Inorg. Chim. Acta 300-302 (2000) 698.
[16] S.I. Gorelsky, A.B.P. Lever, Int. J. Quant. Chem. 80 (2000) 636.
[17] M. Turki, C. Daniel, S. zalis, A. Vlcek, Jr., J. van Slageren, D.J. Stufkens, J. Am. Chem. Soc. 123 (2001) 11431.
[18] M.C. Heitz, C. Daniel, J. Am. Chem. Soc. 119 (1997) 8269.
[19] D. Guillaumont, C. Daniel, J. Am. Chem. Soc. 121 (1999) 11733.
[20] D. Guillaumont, A. Vlcek, Jr., C. Daniel, J. Phys. Chem. A 105 (2001) 1107.
[21] D.J. Tozer, R.D. Amos, N.C. Handy, B.O. Roos, L. Serrano-Andrés, Mol. Phys. 97 (1999) 859.
[22] M.C. Heitz, C. Ribbing, C. Daniel, J. Chem. Phys. 106 (4) (1997) 1421.
[23] B.D. Rossenaar, E. Lindsay, D.J. Stufkens, A. Vlcek, Jr., Inorg. Chim. Acta 250 (1996) 5.
[24] B.D. Rossenaar, D.J. Stufkens, A. Oskam, J. Fraanje, K. Goubitz, Inorg. Chim. Acta 247 (1996) 215.
[25] D.J. Stufkens, A. Vlcek, Jr., Coord. Chem. Rev. 177 (1998) 127.
[26] D.J. Stufkens, J.M.W. van Outerstep, A. Oskam, B.D. Rossenaar, G.J. Stor, Coord. Chem. Rev. 132 (1994) 147.
[27] B.D. Rossenaar, C.J. Kleverlaan, M.C.E. van de Ven, D.J. Stufkens, A. Vlcek, Jr., Chem. A Eur. J. 2 (1996) 228.
[28] I.R. Farrell, P. Matousek, C.J. Kleverlaan, A. Vlcek, Jr., Chem. A Eur. J. 6 (2000) 1386.
[29] M.P. Aarnts, D.J. Stufkens, M.P. Wilms, E.J. Baerends, A. Vlcek, Jr., I.P. Clark, M.W. George, J.J. Turner, Chem. A Eur. J. 2 (1996) 1556.
[30] M.P. Aarnts, D.J. Stufkens, A. Vlcek, Jr., Inorg. Chim. Acta 266 (1997) 37.
[31] D.J. Stufkens, M.P. Aarnts, J. Nijhoff, B.D. Rossenaar, A. Vlcek, Jr., Coord. Chem. Rev. 171 (1998) 93.
[32] J. van Slageren, D.M. Martino, C.J. Kleverlaan, A.P. Bussandri, H. van Willigen, D.J. Stufkens, J. Phys. Chem. A 104 (2000) 5969.
[33] I. Bruand-Cote, C. Daniel, Chem. A Eur. J. (2002), in press.
[34] M.C. Heitz, D. Guillaumont, I. Cote-Bruand, C. Daniel, J. Organomet. Chem. 609 (2000) 66.
[35] M.A. Robb, M. Garavelli, M. Olivucci, F. Bernardi, Rev. Comp. Chem. 15 (2000) 87.